

Generation of scalable many-body Bell correlations in spin chains with short-range two-body interactions

Marcin Płodzień^{1,*}, Tomasz Wasak², Emilia Witkowska,³ Maciej Lewenstein^{1,4} and Jan Chwedeńczuk^{5,†}

¹*ICFO - Institut de Ciències Fòniques, The Barcelona Institute of Science and Technology, 08860 Castelldefels, Barcelona, Spain*

²*Institute of Physics, Faculty of Physics, Astronomy, and Informatics, Nicolaus Copernicus University in Toruń, Grudziądzka 5, 87-100 Toruń, Poland*

³*Institute of Physics PAS, Aleja Lotników 32/46, 02-668 Warszawa, Poland*

⁴*ICREA, Pg. Lluís Companys 23, 08010 Barcelona, Spain*

⁵*Faculty of Physics, University of Warsaw, ul. Pasteura 5, PL-02-093 Warsaw, Poland*



(Received 23 June 2023; accepted 12 March 2024; published 15 April 2024)

Dynamical generation of strong and scalable quantum resources, like many-body entanglement and Bell correlations, in spin-1/2 chains is possible with all-to-all interactions, either for constant interaction strength realizing one-axis twisting protocol or for power-law decaying potentials. We show, however, that such quantum resources can also be dynamically generated with a finite range of interactions. We identify a threshold range and indicate a threshold time when scalable quantum correlations appear. Finally, we show that the certification of generated states is accessible in modern quantum simulator platforms.

DOI: [10.1103/PhysRevResearch.6.023050](https://doi.org/10.1103/PhysRevResearch.6.023050)

I. INTRODUCTION

The potential for future quantum technologies is fuelled by resources [1–3] which are the quantum coherence and the triad of many-body nonclassical correlations: entanglement [4], Einstein-Podolsky-Rosen (EPR) steering [5], and the Bell nonlocality [6]. As such, the main goal of quantum technologies in the next years is generation, characterization, storage, and certification of many-body quantum states [7].

The archetypal model allowing generation of scalable quantum resources is a spin-1/2 chain undergoing one-axis twisting (OAT) [8,9]. In the OAT protocol, the dynamics is governed by a nonlinear Hamiltonian with all-to-all, i.e., infinite-range, spin couplings, while initially spins are polarized along a direction perpendicular to the Hamiltonian axis. The OAT protocol dynamically generates metrologically useful spin-squeezed states [9–12], many-body entangled, and the many-body Bell-correlated states [8,13–34]. It was realized experimentally with ultracold systems utilizing atom-atom collisions [35–38], atom-light interactions [39,40], Rydberg atoms [41–43], arrays of trapped ions [44,45], and superconducting qubits [46–48]. There are theoretical proposals for the OAT simulation with ultracold atoms in optical lattices [31,49–55]. All these proposals are based on the presence of the all-to-all couplings. However, the question of whether such long-range interactions between elementary spins are necessary for scalable quantum resources has been

weakly addressed. Particularly important is the determination of the minimal interaction range and the rate at which the resources are generated.

Here, we attempt to answer this question by focusing on the many-body Bell correlations [23,25,51]. We consider dynamics of spin-1/2 chains governed by an OAT-type Hamiltonian but with finite-range couplings. We find analytically that a minimal range allowing scalable many-body Bell correlations is 4 and is independent of the total number of spins N . We characterize the depth of these correlations as a function of the interaction range, and N , and determine the threshold time at which they emerge. Finally, we show that the dynamically generated quantum states possessing many-body Bell correlations can be certified with the help of present experimental techniques in the state-of-the-art platforms for quantum simulators [43,45,56,57].

This manuscript is organized as follows. In Sec. II we introduce our model and discuss the main properties of the many-body Bell correlator that is well-suited to detect quantum correlations in this system. In Sec. II A we identify the universal interaction range beyond which the Bell correlations are dynamically generated in the spin chain. Next, in Sec. II B we show that there exists a threshold time, scaling inversely with the number of spins, at which the correlations emerge. In Sec. II C we argue that the range of two-body interactions translates onto the strength of Bell correlations, while in Sec. II D we show how these correlations can be efficiently measured with modern experimental techniques. We present some concluding remarks in Sec. III, while some details of analytical calculations are presented in the Appendixes.

II. SPIN CHAINS AND BELL CORRELATIONS

Let us consider a one-dimensional chain of N spins-1/2, with open boundary conditions, described by the

*marcin.plodzien@icfo.eu

†jan.chwedenczuk@fuw.edu.pl

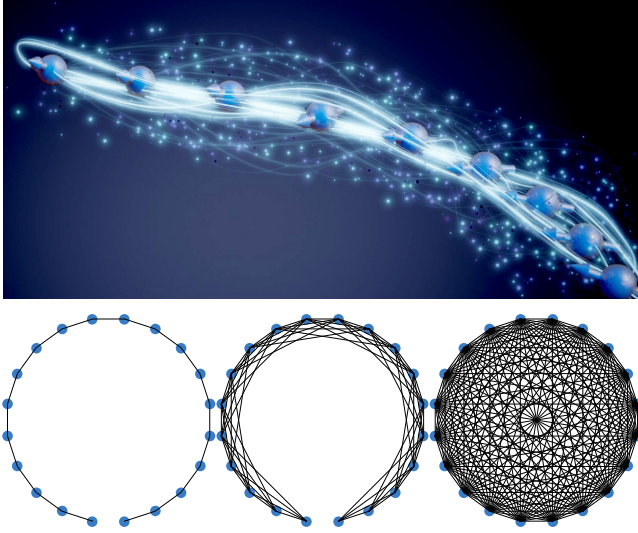


FIG. 1. (Top panel) An illustration of a chain of spins (spheres with arrows) interacting by means of finite-range interactions (lines). (Bottom panel) Visualization of the spin connectivity in a chain of N spins for different interaction ranges r . The three panels show nearest-neighbor interaction with the range $r = 1$ (left), finite-range interaction with $r = 4$ (middle), and the all-to-all type of coupling with $r = N - 1$, present in one-axis-twisting-like protocols (right).

following Hamiltonian:

$$\hat{H} = \sum_{k,l=1}^N J_{kl} \hat{\sigma}_z^{(k)} \hat{\sigma}_z^{(l)}, \quad (1)$$

where J_{kl} is the coupling strength (in units of \hbar) of the k th spin interacting with its l th partner. Here we take the finite-range interaction potential governed by the rectangular function $J_{kl} = 1$ for $0 < |k - l| \leq r$, and 0 otherwise. The range r changes from $r = 1$ (nearest-neighbor couplings) to $r = N - 1$ (all-to-all couplings), see Fig. 1. An experiment [58] showed a high degree of control over the distance-selective interactions J_{kl} .

In the following we consider a dynamical generation of quantum resources, namely, many-body entanglement and many-body Bell correlations. The protocol starts with the uncorrelated spins polarized along the x axis, orthogonal to the z axis distinguished by the Hamiltonian \hat{H} , namely, the initial state for the dynamics is

$$|+1\rangle_x^{\otimes N} = \left[\frac{1}{\sqrt{2}} (|+1\rangle_z + |-1\rangle_z) \right]^{\otimes N}, \quad (2)$$

a so-called spin coherent state, and by $|\pm 1\rangle_x$ we denote an eigenstate of the x -axis Pauli operator with a ± 1 eigenvalue. Next, we evolve the system with the time-evolution operator $\hat{U}(\tau) = e^{-i\tau\hat{H}}$, i.e., the state of the system of spins after time τ is

$$|\psi(\tau)\rangle = \hat{U}(\tau) |+1\rangle_x^{\otimes N}. \quad (3)$$

During the evolution, the two-body interaction in \hat{H} correlates spins. In the limiting case of the all-to-all interactions, $r = N - 1$, the system dynamics is equivalent to OAT, where the many-body entanglement and Bell correlations of

arbitrary depth can be generated [51]. A well-suited tool to address questions posed in the Introduction is the many-body Bell correlator

$$\mathcal{E}_N(\tau) = |\langle \hat{\sigma}_+^{(1)} \cdots \hat{\sigma}_+^{(N)} \rangle|^2. \quad (4)$$

Alternatively, we will use a normalized logarithm of this correlator, namely,

$$Q_N = \log_2(2^N \mathcal{E}_N(\tau)), \quad (5)$$

where the rising operators are taken along the x axis, i.e., $\hat{\sigma}_+^{(k)} = \frac{1}{2}(\hat{\sigma}_y^{(k)} + i\hat{\sigma}_z^{(k)})$ [51]. This choice of orientation is dictated by the observation that the OAT dynamics generates Greenberger-Horne-Zeilinger (GHZ)-type superpositions of $|1\rangle_x^{\otimes N}$ and $|-1\rangle_x^{\otimes N}$ states at time $\tau = \pi/4$.

To see how \mathcal{E}_N relates to the local-hidden-variable (LHV) theory, replace each $\hat{\sigma}_{x/y}^{(k)}$ with a c -number quantity $\sigma_{x/y}^{(k)}$ that can take binary (± 1) values depending on the random hidden variable λ . The locality resides in the assumption that σ 's depend only on a single label k , while realism implies the presence of a probability distribution $p(\lambda)$ for the hidden variable. Hence, a classical counterpart of \mathcal{E}_N consistent with the LHV theory is

$$\mathcal{E}_N^{(\text{LHV})} = \left| \int d\lambda p(\lambda) \sigma_+^{(1)}(\lambda) \cdots \sigma_+^{(N)}(\lambda) \right|^2. \quad (6)$$

Employing now the Cauchy-Schwarz inequality and the fact that for binary outcomes $|\sigma_+^{(k)}(\lambda)|^2 = 1/2$, we obtain the bound $\mathcal{E}_N^{(\text{LHV})} \leq 2^{-N}$, which is the N -body Bell inequality [24]. Note that in Eq. (6) we did not assume that the N subsystems are described by quantum mechanics. If that were the case, the restriction that the quantum spin lies within the Bloch sphere would yield $|\langle \hat{\sigma}_+^{(k)}(\lambda) \rangle|^2 \leq 1/4$, where the mean denotes the trace with the single-qubit density matrix. Hence the violation of the inequality $\mathcal{E}_N \leq 4^{-N}$ implies the presence of entanglement in the system; for details see Ref. [23].

Among these two limiting cases of the structure of the bounds ($\mathcal{E}_N \leq 4^{-N}$ and $\mathcal{E}_N \leq 2^{-N}$), there is a large set of inequalities obtained under assumptions of quantum-mechanical restrictions for some subset of N parties.

Note that the violation of the Bell inequality $\mathcal{E}_N > 2^{-N}$, or equivalently, $Q_N > 0$ [see Eq. (5)], ensures entanglement and the EPR steering in the system [5]. To summarize, $\mathcal{E}_N^{(\text{LHV})}$ from Eq. (6) is consistent with the LHV theory and hence sets the Bell limit. The correlator \mathcal{E}_N from Eq. (4) is its quantum equivalent, designed to witness nonclassical correlations in many-body systems. Furthermore, large \mathcal{E}_N implies strong Bell correlations. To see this, take the maximally nonclassical state, the GHZ state $|\psi_{\text{GHZ}}\rangle = \frac{1}{\sqrt{2}}(|+1\rangle_x^{\otimes N} + |-1\rangle_x^{\otimes N})$, which gives the largest value of the Bell correlator (4), i.e., $\mathcal{E}_N = \frac{1}{4}$, or more conveniently for this purpose, $Q_N = N - 2$ [see the right-hand side of Eq. (4)]. If a single spin is correlated to the remaining quantum state of $N - 1$ spins by a LHV theory, similarly to Eq. (6), we obtain the maximal value of $Q_N = N - 3$. Hence, $Q_N > N - 3$ implies that the nonlocality encompasses all the spins, and we say that the nonlocality depth, denoted with ν , is $\nu = N$. These considerations can be generalized to other integer values of Q_N , and when

$$\nu - 3 < Q_N \leq \nu - 2, \quad (7)$$

then up to ν spins are Bell correlated. For further analysis we introduce the fraction of the Bell-correlated particles defined as $\beta = Q_N/N$. For more on nonlocality depth and the related depth of entanglement, see Refs. [19–24,59].

A. Universal threshold interaction range

In the following we find an N -independent threshold range r allowing for the generation of Bell correlations witnessed by \mathcal{E}_N during unitary time evolution, Eq. (3). First, we note that in general, the exact numerical calculation of the correlator in Eq. (4) is exponentially hard, as it requires working in the full many-body basis of dimension 2^N with access to the N -body operator $\hat{\sigma}_+^{(1)} \cdots \hat{\sigma}_+^{(N)}$. However, in the considered scenario where $[\hat{H}, \hat{\sigma}_z^{(k)}] = 0$, as we have found, Eq. (4) with Eq. (3) can be exactly and with no approximations expressed as

$$\mathcal{E}_N(\tau) = \left| 2^{-2N} \sum_{\sigma, \sigma'} e^{-i\tau(H_\sigma - H_{\sigma'})} \sigma_1 \cdots \sigma_N \right|^2, \quad (8)$$

where $H_\sigma = \sum_{k,l=1}^N J_{kl} \sigma_k \sigma_l$, and the sum runs over the vectors of eigenvalues of $\hat{\sigma}_z^{(k)}$ operators, i.e., $\sigma = (\sigma_1, \dots, \sigma_N)$ and $\sigma' = (\sigma'_1, \dots, \sigma'_N)$, over 2^N combinations of $\sigma_1, \dots, \sigma_N$ and $\sigma'_1, \dots, \sigma'_N$, which take values of ± 1 . The formula in Eq. (8) allows for the *exact* calculation of the Bell correlator for the high number of qubits (here up to $N = 300$), since the exponentially growing dimensionality of the Hilbert space is no longer a computational constraint (for derivation details see Appendix A).

Let us consider first the marginal cases. For the aforementioned range $r = 1$, the Bell correlator is given by the analytical formula $\mathcal{E}_N(\tau) = \sin^N(\tau) \cos^{3N-4}(\tau)$. This expression has a maximum $\max_\tau(\mathcal{E}_N) \approx 2^{-1.6N+1}$ at $\tau \simeq \pi/6$, which is exponentially smaller than the Bell limit 2^{-N} . Equivalently, $Q_N = -0.6N + 1$, and the deviation from the Bell limit $Q_N = 0$ becomes larger with N . Therefore, the nearest-neighbor interactions cannot generate many-body Bell correlations in our case. The other extreme case is the all-to-all interactions with $r = N - 1$, which was considered in detail in [51]. This case realizes the OAT protocol, and the Bell correlations are present from $\tau \simeq 1.5/N$. At $\tau = \pi/4$, the N -body GHZ state is formed [50,54,55], and the correlator in Eq. (4) reaches its maximal value $\mathcal{E}_N = 1/4$, which is exponentially larger than the bound in the N -body Bell inequality.

In Figs. 2(a)–2(d) we present the time evolution of the correlator $Q_N(\tau)$, calculated using Eq. (8), for different intermediate ranges $1 \leq r \leq 5$ and for all-to-all couplings $r = N - 1$ for various spin numbers $N = 64$ (panel a), 128 (b), 256 (c), and 300 (d). We observe that the correlator only breaks the Bell limit $Q_N > 0$ when $r \geq 4$ even for large N . This is the first indication of the presence of a threshold range. However, it must be verified whether the value of $r = 4$ is universal, i.e., independent of the system size. To this end, we focus on

$$Q_N^{\max} \equiv \max_\tau Q_N(\tau), \quad (9)$$

i.e., maximized Q_N with respect to τ calculated for different N 's. In Fig. 2(e) we show Q_N^{\max} as a function of the number of spins N and for various values of $1 \leq r \leq 5$. For a

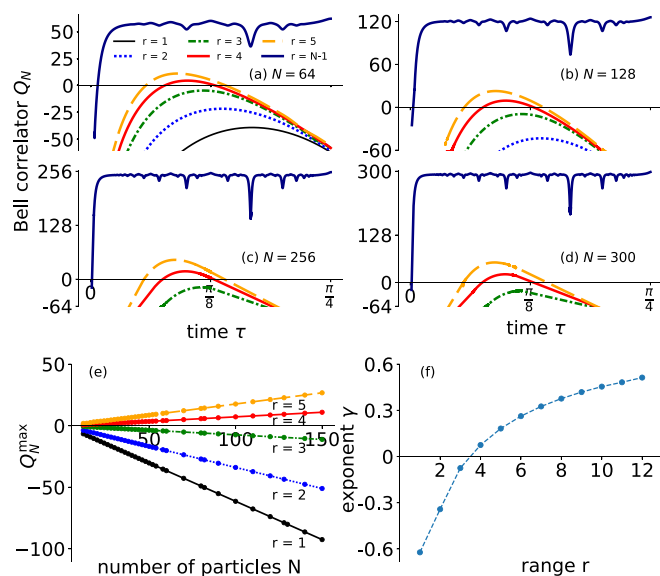


FIG. 2. (a)–(d) The Bell correlator $Q_N(\tau)$ for $N = 64, 128, 256, 300$ spins as a function of time τ for the interaction range: $r = 1$ (thin-solid-black), $r = 2$ (dotted-blue), $r = 3$ (dashed-dotted-green), $r = 4$ (thick-solid-red), $r = 5$ (dashed-orange) and $r = N - 1$ (solid-dark-blue). The values $Q_N > 0$ mark the region where the many-body Bell inequality is violated. (e) The first maximum of Q_N with respect to time, Q_N^{\max} , as a function of the total number of spins N for various $r \in [1, 5]$. (f) The exponent of the Bell correlator in the scaling with N , approximated as $Q_N^{\max} \approx \gamma N + \text{const}$, or, equivalently, $2^N \max_\tau \mathcal{E}_N(\tau) \propto 2^{\gamma N}$. The growth of scalable many-body Bell correlations with N is manifested by positive γ when $r \geq 4$.

given r and large N , these maximal values lie on a straight line determining an exponent γ in the exponential scaling of $\mathcal{E}_N \propto 2^{(\gamma-1)N}$. In Fig. 2(f) we present the value of γ as a function of the interaction range. For $r \geq 4$ we find positive exponents indicating that the degree of the Bell inequality violation becomes higher with growing N , in contrast to the case of $r \leq 3$. Therefore the change in the sign of γ indicates qualitatively different scaling regimes of the Bell correlations.

The observed behavior of Q_N^{\max} and $\gamma(r) > 0$ for $r \geq 4$ demonstrates that $r = 4$ is indeed a *threshold range* at which the Bell correlations are detected. Crucially, Q_N^{\max} increases with growing N , indicating scalable Bell correlations in this system [24]. Remarkably, although $r = 4$ in the limit $N \gg 1$ is a short-range interaction encompassing an intensive number of neighboring spins, the system still exhibits an increasing degree of violation of the Bell inequality with increasing system size. The invariance of the threshold range with respect to the number of spins proves its universality.

Qualitatively, the strengthening of Bell correlations with growing r can be explained as follows. To generate the GHZ-like coherence, which is the witness of Bell correlations [see Eq. (4)], one needs to flip all the spins and, hence, to act with an N -body operator $\hat{B}_N = \hat{\sigma}_z^{(1)} \cdots \hat{\sigma}_z^{(N)}$ on the input state, since $\hat{\sigma}_z | + 1 \rangle_x = | - 1 \rangle_x$. Note that the evolution operator coupling any pair of spins is $e^{-i\tau \hat{\sigma}_z^{(k)} \hat{\sigma}_z^{(l)}} = \cos(\tau) - i \sin(\tau) \hat{\sigma}_z^{(k)} \hat{\sigma}_z^{(l)}$. As r grows, each spin couples to more neighbors, and the number of possible combinations of interacting terms giving the operator \mathcal{B}_N grows

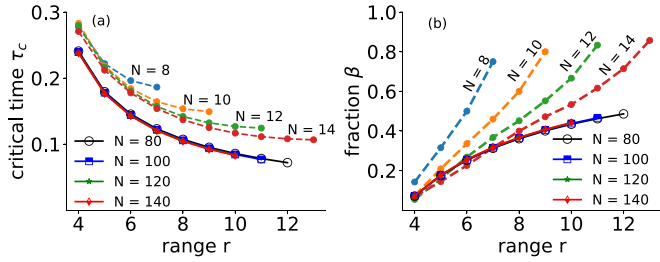


FIG. 3. (a) The threshold time τ_c at which the Bell correlator passes the Bell limit, $Q_N = 0$, as a function of interaction range r . The dashed curves correspond to the limit $r \lesssim N$, while solid curves correspond to the limit $r \ll N$. The latter collapses onto the same line. (b) The maximal fraction of correlated spins $\beta = \nu/N$ as a function of range r , see Eq. (7).

exponentially, consequently increasing $\mathcal{E}_N(\tau)$. This growth is, however, balanced by the exponential decay of the amplitude of the initial state. The eventual observation of the Bell inequality violation is, thus, the effect of the competition between the two indicated mechanisms. In order to formalize these observations, we developed the spin-inversion asymptotic expansion theory; for quantitative explanations using a diagrammatic approach¹ and the details on the asymptotic theory, see Appendix B.

B. Threshold time

As evident from Figs. 2(a)–2(d), the interaction range r determines the threshold time τ_c , at which Bell correlations emerge. This dependence can be extracted from Eq. (8) as follows. For an arbitrary internal spin coupled with $2r$ neighbors, the sum over $\sigma_k = \pm 1$ vanishes unless the corresponding phase term $e^{-i\tau\sigma_k(\sigma_{k-r} + \dots + \sigma_{k+r})}$ oscillates quickly enough. The sum in the parenthesis is at most equal to $2r$, and hence the phase factor will vary significantly between $\sigma_k = -1$ and $\sigma_k = 1$ if $\tau \cdot 2r \gtrsim 1$. Thus, the Bell correlator becomes significantly nonzero if $\tau_c \gtrsim a/r$, where a is some constant. The scaling of τ_c , which is inversely proportional to the interaction range, is confirmed by exact solution of the dynamics generated by Eq. (1). In Fig. 3(a) we identify the threshold time τ_c when Q_N surpasses the Bell limit for different values of large $N = 80, 100, 120, 140$, for which $r \ll N$ and small $N = 8, 10, 12, 14$, where $r \lesssim N$. The observed behavior shows that for large systems, τ_c becomes independent of the system size. By changing r from the threshold value $r = 4$ to $r = N = 14$ we recover the scaling $\tau_c \propto 1/N$ characteristic to the all-to-all coupling case [51].

C. Fraction of Bell-correlation spins

In Fig. 3(b) we present the dependence of the fraction of Bell-correlated spins $\beta = \nu/N$ as a function of the range r , deduced from Q_N^{\max} , see Eq. (7). In the limit of $N \gg r$, the results follow the universal curve. This can be understood as

¹For intermediate values of r , in our open-access repository [95] we provide examples of the time evolution of $\mathcal{E}_N(\tau)$ obtained analytically for concrete values of N and r .

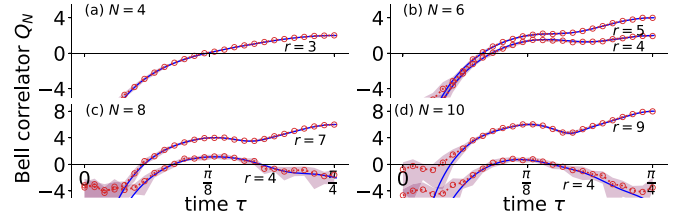


FIG. 4. The dynamics of the estimated many-body Bell correlator Q_N for (a) $N = 4$, (b) $N = 6$, (c) $N = 8$, and (d) $N = 10$ spins with interaction range $r = 4$ (lower curves), and all-to-all connections $r = N - 1$ (upper curves). Solid blue lines present exact results, while red circles represent the value of the reconstructed many-body Bell correlator from the classical shadows tomography. Standard deviation is marked as a shaded area.

follows. Using the asymptotic exponential scaling for large N , i.e., $Q_N \approx \gamma(r)N$ [see the discussion below Eq. (9)], we can estimate the nonlocality depth by $\nu_N \approx Q_N$ up to corrections on the order of $1/N$. Then, the fraction $\beta \approx \gamma(r)$, which shows that for large N , β becomes independent of N , as is observed in the figure. This relation uncovers the physical role of the exponent of \mathcal{E}_N as a concentration of Bell-correlated particles. Therefore, we find the range not only controls the threshold time τ_c , but also the number of Bell-correlated clusters in the system.

D. Many-body Bell-correlation certification

Measuring higher-order quantum correlations is challenging. However, the many-body correlations considered here can be certified by inspecting only one element of the density matrix, which couples the state with all spins up, with the state with all spins down in the x basis, see Eq. (4). As such, the problem of many-body Bell-correlation measurement can be cast as a quantum-state tomography task [60–76].

With the full many-body calculations, we simulated tomographical reconstruction of the density matrix with classical shadows tomography [77–86], which was employed for trapped ions [87–89] and Rydberg atom arrays [90]. We prepared ten reconstructions of the target density matrix $\hat{\rho}(\tau)$ at a given time τ , where each reconstruction consists of M classical shadows. From each reconstructed $\hat{\rho}(\tau)$ we extracted the Bell correlator, and based on the generated collection, we estimated the mean and standard deviation of the reconstruction $\mathcal{E}^*(\tau) \equiv 2Q_N^*(\tau)^{-N}$. In Fig. 4 we demonstrate that Bell correlations quantified by $Q_N(\tau)$ (solid blue lines) can be successfully certified by the tomographically reconstructed mean value $Q_N^*(\tau)$ (red circles) with standard deviation (shaded areas) for $N = 4, 6, 8, 10$ spins with the interaction range $r = 4$, and the all-to-all couplings when $r = N - 1$. We prepared a $M = 10^5 N$ classical shadow for $N = 10$ and $r = 4$, and $M = 10^4 N$ otherwise.

An alternative method to measure considered Bell correlations relies on the multiple quantum coherences [91,92], see Appendix C.

III. DISCUSSION AND CONCLUSIONS

We showed that all-to-all spin couplings are not necessary and that an OAT-type Hamiltonian with finite-range interactions only is sufficient to efficiently generate scalable, many-body entanglement and Bell correlations, which can be measured with classical shadows tomography or multiple quantum coherences measurements.

Recently, preparation of spin-squeezed states on variational quantum circuits was proposed [93]. On the other hand, our results have important consequences for digital quantum computers, aiming to generate scalable many-body entanglement and Bell correlations dynamically. In a single trotterization step of the OAT the number of two-qubit entangling gates scales quadratically with the number of qubits [46–48,94], while for the finite-threshold-range interactions considered here, it scales linearly.

The data presented in this article is available from [96].

ACKNOWLEDGMENTS

We acknowledge discussion with A. Safavi-Naini, R. Gerritsma, R. Blatt, and T. Roscilde. J.Ch. was funded by the National Science Centre, Poland, within the QuantERA II Program that has received funding from the European Union's Horizon 2020 Research and Innovation Program under Grant Agreement No. 101017733, Project No. 2021/03/Y/ST2/00195. E.W. acknowledges support from the DAINA project of the Polish National Science Center DEC-2020/38/L/ST2/00375. This research is part of the project No. 2021/43/P/ST2/02911 co-funded by the National Science Centre and the European Union Framework Programme for Research and Innovation Horizon 2020 under the Marie Skłodowska-Curie grant agreement No. 945339. For the purpose of open access, the author has applied a CC-BY public copyright licence to any author accepted manuscript (AAM) version arising from this submission. The ICFO group acknowledges support from ERC AdG NOQIA; Ministerio de Ciencia y Innovation Agencia Estatal de Investigaciones (PGC2018-097027-B-I00/10.13039/501100011033, CEX2019-000910-S/10.13039/501100011033, Plan Nacional FIDEUA PID2019-106901GB-I00, FPI, QUANTERA MAQS PCI2019-111828-2, QUANTERA DYNAMITE PCI2022-132919, Proyectos de I+D+I "Retos Colaboración" QUSPIN RTC2019-007196-7); MICIIN with funding from European Union Next Generation EU (PRTR-C17.I1) and by Generalitat de Catalunya; Fundació Cellex; Fundació Mir-Puig; Generalitat de Catalunya (European Social Fund FEDER and CERCA program, AGAUR Grant No. 2021 SGR 01452, QuantumCAT U16-011424, cofunded by the ERDF Operational Program of Catalonia 2014-2020); Barcelona Supercomputing Center MareNostrum (FI-2022-1-0042); EU (PASQuaS2.1, 101113690); EU Horizon 2020 FET-OPEN OPTologic (Grant No 899794); EU Horizon Europe Program (Grant Agreement No. 101080086 – NeQST), National Science Centre, Poland (Symfonia Grant No. 2016/20/W/ST4/00314); ICFO Internal "QuantumGaudi" project; and the European Union's Horizon 2020 Research and Innovation Program under

Marie-Skłodowska-Curie Grant Agreement No. 101029393 (STREDCH). M.P. acknowledges the support of the Polish National Agency for Academic Exchange, the Bekker Program No. PPN/BEK/2020/1/00317. Views and opinions expressed are, however, those of the author(s) only and do not necessarily reflect those of the European Union, European Commission, European Climate, Infrastructure and Environment Executive Agency (CINEA), nor any other granting authority. Neither the European Union nor any granting authority can be held responsible for them.

M.P. indicated the existence of the threshold interaction range, performed many-body simulations, analytical calculations in Ref. [95], and quantum-state tomography results. J.Ch. prepared analytical expressions for the Bell correlator, threshold range, and threshold time, and performed many-body calculations. T.W. developed the spin-inversion asymptotic expansion theory and performed many-body calculations. All the authors contributed to discussing the results and the manuscript preparation and revision.

APPENDIX A: APPENDIX ON DERIVATION OF EQ. (8)

We begin by invoking a general expression for the density matrix of N qubits, which is

$$\hat{\rho}_{\text{in}} = \sum_{\sigma, \sigma'} \rho_{\sigma, \sigma'} |\sigma\rangle_{zz} \langle \sigma'|, \quad (\text{A1})$$

where

$$\hat{\sigma}_z^{(k)} |\sigma\rangle_z = \sigma_k |\sigma\rangle_z, \quad (\text{A2})$$

and the double sum over σ and σ' is a shortened notation for $2N$ sums over $\sigma_1, \dots, \sigma_N = \pm 1$ and $\sigma'_1, \dots, \sigma'_N = \pm 1$. Since the Hamiltonian contains only $\hat{\sigma}_z^{(l)}$ operators, it is natural to use as the basis the product of eigenstates of N z -axis Pauli matrices. Hence, the action of the evolution operator on each such ket is formally equivalent to replacing all Pauli operators in Eq. (1) with a corresponding set of σ numbers, i.e.,

$$e^{-i\hat{H}\tau} |\sigma\rangle_z = e^{-i\tau \sum_{k,l=1}^N \hat{\sigma}_z^{(k)} \hat{\sigma}_z^{(l)}} |\sigma\rangle_z \equiv e^{-i\tau H_\sigma} |\sigma\rangle_z. \quad (\text{A3})$$

Therefore, the output state becomes

$$\hat{\rho}_{\text{out}}(\tau) = e^{-i\tau\hat{H}} \hat{\rho}_{\text{in}} e^{i\tau\hat{H}} = \sum_{\sigma, \sigma'} e^{-i\tau(H_\sigma - H_{\sigma'})} \rho_{\sigma, \sigma'} |\sigma\rangle_{zz} \langle \sigma'|. \quad (\text{A4})$$

Since the correlator \mathcal{E}_N is calculated with the product of N operators raising the spin projection along the x axis, it is convenient to change the basis using

$$\begin{bmatrix} | + 1_k \rangle_z \\ | - 1_k \rangle_z \end{bmatrix} = \frac{\hat{\sigma}_x^{(k)} + \hat{\sigma}_z^{(k)}}{\sqrt{2}} \begin{bmatrix} | m_k = +1 \rangle_z \\ | m_k = -1 \rangle_z \end{bmatrix}, \quad (\text{A5})$$

where $\frac{\hat{\sigma}_x^{(k)} + \hat{\sigma}_z^{(k)}}{\sqrt{2}}$ is the so-called Hadamard matrix. Equation (A5) can be equivalently expressed as

$$|\sigma_k\rangle_z = \frac{1}{\sqrt{2}} \sum_{m_k = \pm 1} \sigma_k^{\frac{1-m_k}{2}} |m_k\rangle_x, \quad (\text{A6})$$

$\sigma_k = \pm 1$, where the right-hand side is expressed in the eigenbasis of x -axis Pauli operators. Substituting this result into

Eq. (A4), we obtain

$$\hat{\rho}_{\text{out}}(\tau) = \frac{1}{2^N} \sum_{\sigma, \sigma'} e^{-i\tau(H_\sigma - H_{\sigma'})} \rho_{\sigma, \sigma'} \times \sum_{m, m'} |m\rangle_{xx} \langle m'| \prod_{k=1}^N \sigma_k^{\frac{1-m_k}{2}} \sigma_k'^{\frac{1-m'_k}{2}}, \quad (\text{A7})$$

where the vector $\mathbf{m} = (m_1, \dots, m_N)$, and $\hat{\sigma}_x^{(k)} |\mathbf{m}\rangle_x = m_k |\mathbf{m}\rangle_x$. The correlator couples the two extreme elements of the density matrix: the one where all spins are up, $|+1\rangle_x^{\otimes N}$, with that where all are down, $|-1\rangle_x^{\otimes N}$. Hence it can be expressed by a single element of $\hat{\rho}_{\text{out}}(\tau)$, namely, the coherence term between these two elements. By setting all m 's to -1 and all (m')'s to $+1$, we get

$$\mathcal{E}_N = |{}_x \langle +1 |^{\otimes N} \hat{\rho}_{\text{out}}(\tau) | -1 \rangle_x^{\otimes N}|^2 = \left| \frac{1}{2^N} \sum_{\sigma, \sigma'} e^{-i\tau(H_\sigma - H_{\sigma'})} \rho_{\sigma, \sigma'} \sigma_1 \cdots \sigma_k \right|^2, \quad (\text{A8})$$

as invoked in Eq. (8) of the main text for the case of the input state Eq. (3), which yields $\rho_{\sigma, \sigma'} = 2^{-N}$.

APPENDIX B: DIAGRAMMATIC SPIN-INVERSION ASYMPTOTIC EXPANSION THEORY

To capture the physical mechanism of the correlations' enhancement beyond the universal threshold range $r = 4$, we resort to an asymptotic diagrammatic expansion of the many-body state coefficients in the number of spin inversions throughout the evolution. The proposed method provides information about the time dependence of \mathcal{E}_N , enabling the estimation of the threshold time and indicating the origin of enhanced correlation at the threshold range $r = 4$.

We consider first the part of the Hamiltonian from Eq. (1), which couples a single pair, i.e., $\hat{H}_{kl} = J_{kl} \hat{\sigma}_z^{(k)} \hat{\sigma}_z^{(l)}$. Then, under the action of \hat{H}_{kl} , we obtain

$$e^{-i\tau \hat{H}_{kl}} |1_k\rangle_z |1_l\rangle_z = \hat{f}_{kl} |1_k\rangle_z |1_l\rangle_z, \quad (\text{B1})$$

where $\hat{f}_{kl} = \cos(J_{kl}\tau) - i \sin(J_{kl}\tau) \hat{\sigma}_z^{(k)} \hat{\sigma}_z^{(l)}$. The action of the second term in the operator \hat{f}_{kl} inverts the spins due to the property $\hat{\sigma}_z^{(k)} |1_k\rangle_z = |-1_k\rangle_z$ unless the distance $d = |k - l|$ exceeds the range r . Since the evolution of the state is given by a product of the terms from Eq. (B1),

$$|\psi(\tau)\rangle = \prod_{k,l} \hat{f}_{kl} | +1 \rangle_x^{\otimes N}, \quad (\text{B2})$$

we can represent the final state diagrammatically as a sequence of dots (each corresponding to the initial state of the individual spin) and lines connecting pairs of dots. To each line connecting a pair we assign either the amplitude $\cos(\tau)$ and an unchanged state of the pair, or the amplitude $-i \sin(\tau)$ to a pair with inverted spins.

The final state is the sum over all possible assignments to all the lines and all possible ways of connecting the pairs of spins that are compatible with the distance of the interaction. In such a case the nontrivial lines can connect only points that are not further apart than the distance r , and there are in total $K \equiv r(2N - r - 1)/2$ of such lines. We now apply this

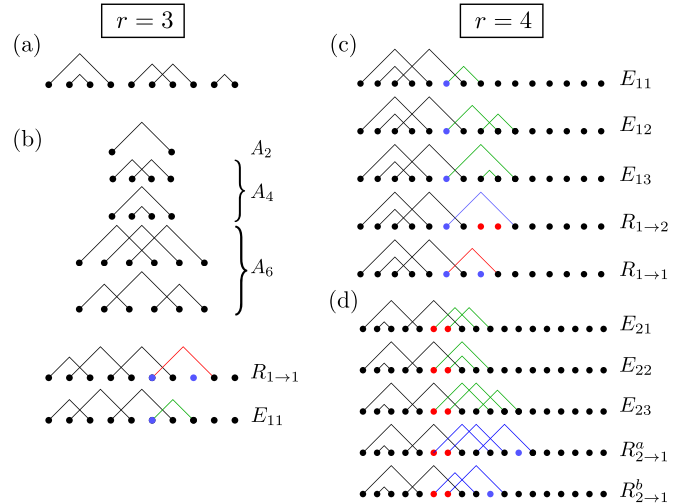


FIG. 5. (a) An example of diagrams for $r = 3$ and $N = 10$. Three disconnected cluster diagrams are visible. (b) The classes of clusters including 2, 4, and 6 spins ($A_{2,4,6}$) for $r = 3$. $R_{x \rightarrow y}^{a/b}$ and E_{xy} with $x, y = 1, 2, 3$ mark extended and closing cluster diagrams as explained in the main text. (c), (d) The classes of cluster diagrams with one (two) unconnected spins are marked with blue (red) points. The green lines close the cluster, and the blue lines exchange the classes between one and two unconnected last spins. The red line extends the diagram within the same class.

diagrammatic method to calculate the \mathcal{E}_N at short times and identify at which r the correlator crosses the Bell limit.

a. Diagrammatic approach

Here we describe the diagrammatic method allowing for physical insights regarding the origin of the threshold interaction range $r = 4$. We begin by analyzing the number of possibilities of forming the diagrams P_r for small values of r . We show that the number of diagram classes in the case of $r = 4$ exceeds those of $r = 3$. As a result, new additional diagrams appear for $r = 4$, which describes a correlation that spreads over the whole chain and thus increases the exponent of $P_4(N)$.

To proceed, we first investigate the case $r = 3$, see Fig. 5(a). As can be seen from the diagram, which is an example for $N = 10$, there are clusters or blocks of spins between which there are no lines. The positions of such different clusters can be exchanged, leading to an exponential scaling with N due to many permutations when N grows. These clusters, including $k = 2, 4$, and 6 spins, which form classes $A_{2,4,6}$, see Fig. 5(b), can appear anywhere in the chain.

For comparison, in the case $r = 1$ only a single class A_2 from Fig. 5(b) contributes, which contains just a single element. As a result, there are $(N/2)!$ such permutations built from the same diagram, and thus $P_1 = (N/2)!/(N/2)! = 1$. In the case $r = 2$, in addition to class A_2 from Fig. 5(b) contributes. Here, we can perform the summation analytically and, after straightforward calculations, we obtain $P_2(N) = F_{N/2+1}$, where F_n is the n th Fibonacci number. For large N we have $P_2 \propto e^{\ln \phi N/2}$, which confirms the exponential scaling with the exponent $(\ln \phi)/2 \approx 0.241$ determined by the golden ratio ϕ .

Importantly, in the case of $r = 3$ there is a single cluster diagram, the class denoted by $R_{1 \rightarrow 1}$ in Fig. 5(b), which can be extended up to arbitrary $k \leq N$ spins by adding a single line shown in red starting from the blue point. The notation $R_{p \rightarrow q}$ is meant to denote a recursive type of diagram that brings p open points to q open points in the cluster. This extended cluster diagram can be terminated at any point by adding the green line as shown in the diagram denoted by E_{11} . Interestingly, such a cluster can include all spins. The appearance of such extended diagrams increases the exponent of P_r to 0.427, which we found by a simple fit, and so approximately by a factor of 2 compared to the case $r = 2$. This increase, however, is insufficient to reach the Bell limit.

For the case $r = 4$, the situation changes qualitatively. Similarly to the $r = 3$ case, small cluster diagrams appear in the expansion, but now the class of extended diagrams is much larger. In Fig. 5(b) we show examples of diagrams which end with one unbound spin (blue). Not only can the cluster be closed by adding one of the green lines from classes $E_{1,j}$ with $j = 1, 2, 3$, but also it can be further extended by using the red line from class $R_{1 \rightarrow 1}$. Alternatively, the diagram can be converted to a cluster ending with two spins, as in class $R_{1 \rightarrow 2}$. Next, such diagrams can be closed [using green lines from classes $E_{2,1/2/3}$ in panel (c)], or converted to a diagram with one unbound spin [as in panel (b)], by using blue lines from class $R_{2 \rightarrow 1}^{a/b}$. As a consequence, by fitting an exponential, we find 0.563 for the exponent P_4 . For completeness, we mention that we found the exponent to be 0.670 for $r = 5$.

The increase of the exponent of $P_4(N)$, relative to the $r = 3$ case, is sufficient to surpass the Bell limit. Such long-range cluster diagrams have a much larger contribution in the case $r = 4$ than for $r = 3$. For instance, for $N = 10$ there are 15 different cluster diagrams embodying all the N spins for $r = 4$ compared to a single diagram for $r = 3$. As a result, the rate of increasing $P_r(N)$ as a function of N is larger with increasing r and leads to crossing the Bell correlations limit when $r = 3$ is increased to $r = 4$.

b. Expansion of correlator \mathcal{E}_N

The correlator $\mathcal{E}_N(\tau)$ from Eq. (3) can be conveniently rewritten in the form

$$\mathcal{E}_N(\tau) = |C_+(\tau)|^2 |C_-(\tau)|^2, \quad (\text{B3})$$

for the pure state from Eq. (B2), where C_+ (C_-) is the amplitude of finding all spins up (down) along the x axis. Therefore, in order to calculate the amplitude C_- , we need to count all the processes that lead to the spin inversion of all N spins, and in order to obtain C_+ we have to take into account all the processes that resulted in no net spin inversion of the initial state. Our approach is to consider only those diagrams in which each spin inverted the fewest number of repetitions, which is justified for short times.

We first determine $C_-(\tau)$, focusing on the dominating process where all the spins have inverted only once. Diagrammatically, each pair of points is connected only once with a line with the amplitude $-i \sin \tau$, and there are $N/2$ such lines, while all the remaining $K - N/2$ lines have amplitudes $\cos \tau$. Therefore, the coefficient C_- is given by

$$C_- \approx P_r(N) (\cos \tau)^{K-N/2} (-i \sin \tau)^{N/2}, \quad (\text{B4})$$

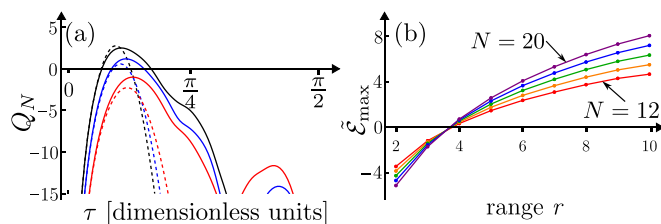


FIG. 6. (a) The comparison of exact (solid) and approximate (dashed) numerics for $N = 16$ and $r = 3$ (red), 4 (blue), 5 (black). The parameters used are $(P_r, R_r) = (491, 40)$ for $r = 3$, $(3116, 76)$ for $r = 4$, and $(12483, 120)$ for $r = 5$. (b) The behavior of \mathcal{E}_{\max} as a function of the range r for various values of $N = 12, 14, 16, 18, 20$. The solid line is a guide to the eye. The value of \mathcal{E}_{\max} is positive for $r = 4$, which signals the existence of τ_{crit} for the Bell inequality violation as given by Eq. (B10).

where $P_r(N)$ denotes the number of possibilities of forming the diagrams.

A similar expansion holds for C_+ , but now we count the diagrams with the least number of lines with the amplitude $-i \sin \tau$, which results in no net spin inversion. In the zeroth order, no spin inversions occur, resulting in the scaling of $\cos^K \tau$. In the first order, such diagrams contain three lines where the three spins i, j , and k are mutually connected and subject to the constraint that all the distances between the pairs fall within the range of the interaction. By the symbol $R_r(N)$, we denote the number of such diagrams for the given range r and the number of spins N . We thus arrive at the following expression:

$$C_+ \approx (\cos \tau)^K + R_r(N) (\cos \tau)^{K-3} (-i \sin \tau)^3. \quad (\text{B5})$$

For $r = 1$ we have only a single diagram with only nearest-neighbors being connected, and thus $P_{r=1} = 1$ and $R_{r=1} = 0$. As a result, we recover the exact formula cited in the main text, namely,

$$\mathcal{E}_N(\tau) = \sin^N(\tau) \cos^{3N-4}(\tau). \quad (\text{B6})$$

For small values of r or N , the actual numbers for P_r and R_r can be found by counting the number of permutations or from analytical solutions [95]. In the large N limit, R_r scales linearly with N , and P_r scales exponentially with an r -dependent exponent. This exponential growth of P_r with a sufficiently large exponent is responsible for surpassing the Bell limit and observation of nonlocal correlations.

In Fig. 6(a) we compare our asymptotic expansion of \mathcal{E}_N from Eq. (B3), calculated with Eq. (B4) and Eq. (B5) for $N = 16$ and the range $r = 3$ (red), 4 (blue), 5 (black). From these examples we see that the proposed approach via the asymptotic spin-inversion expansion works sufficiently well for the correlator \mathcal{E}_N , as it captures the short-time behavior as well as the approximate time of crossing the Bell limit for $r \geq 4$. For $r = 3$ the theory quantitatively shows that the limit is not surpassed.

c. Gaussian approximation

To gain further insight into the expansion method, we approximate the powers of cosines by Gaussian functions, sines

with the first order in τ , and $K - 3 \approx K$ in the second term of $|C_+|^2$, which is valid for large N . In this way we obtain

$$|C_-|^2 \approx P_r^2 \tau^N e^{-(K-N/2)\tau^2}, \quad (\text{B7})$$

$$|C_+|^2 \approx e^{-K\tau^2} (1 + R_r^2 \tau^6). \quad (\text{B8})$$

Furthermore, in the region of τ where the Bell inequality is violated, and around the maximum of \mathcal{E}_N , we can neglect the first term in $|C_+|^2$, which yields our intermediate-time approximation,

$$\mathcal{E}_N \approx P_r^2 R_r^2 e^{-\beta_N \tau^2} \tau^{N+6}, \quad (\text{B9})$$

where we introduced the exponent $\beta_N = 2K - N/2$.

Now we estimate the time of crossing the Bell limit, and, as a result, we show that the approximate expression in Eq. (B9) describes the observed numerical behavior, i.e., that for $r = 3$ the Bell threshold is not surpassed and for $r \geq 4$ we observe the violation of the inequality. However, our approach, being asymptotic in nature, does not accurately capture the threshold time τ_c , where the Bell limit is surpassed, due to its systematic underestimation that manifests in a small offset. In Fig. 6 this offset is not visible, but it can be larger for larger values of r .

To determine τ_c , we expand $\ln(2^N \mathcal{E}_N)$ around the maximum, which is reached at the time $\tau_{\max} = \sqrt{(N+6)/(2\beta_N)}$, up to quadratic terms in $\tau - \tau_{\max}$. The Bell limit $\mathcal{E}_N = 1/2^N$ is reached at

$$\tau_c \approx \tau_{\max} - \sqrt{\frac{\tilde{\mathcal{E}}_{\max}}{2\beta_N}}, \quad (\text{B10})$$

which is meaningful, i.e., $\tau_c \in \mathbb{R}$, only when $\tilde{\mathcal{E}}_{\max} \geq 0$, and where the maximum of the scaled logarithm is

$$\frac{\tilde{\mathcal{E}}_{\max}}{N} = \frac{2 \ln(P_r R_r)}{N} - \left(1 + \frac{6}{N}\right) \ln \frac{1}{\tau_{\max}} + \ln 2 - \frac{1 + \frac{6}{N}}{2}. \quad (\text{B11})$$

Due to the linear scaling of R_r with N , the first term on the right-hand side extracts the exponent of P_r in the first approximation. The second term, which decreases $\tilde{\mathcal{E}}_{\max}$, comes from the factor τ^N in the expansion of C_- originating from the requirement that all the N spins have to be inverted during the dynamics. In Fig. 6(b) we present the function $\tilde{\mathcal{E}}_{\max}$ as a function of the range r for various N 's. The time τ_{crit} from Eq. (B10), when the Bell threshold is reached by \mathcal{E}_N , exists if $\tilde{\mathcal{E}}_{\max} \geq 0$. We find that for $r \leq 3$, $\tilde{\mathcal{E}}_{\max}$ is negative and for $r \geq 4$ it is positive, resulting in a physically meaningful τ_c .

Physically, $\mathcal{E}_N(\tau)$ quantifies how fast the initial state, given by $|C_+(\tau)|^2$, is depleted, and in order to surpass the Bell

inequality, the state with all the spins inverted, given by $|C_-(\tau)|^2$, has to be populated fast enough. The population in $|C_-|^2$ is exponentially enhanced as r increases due to a larger number of diagrams with spin pairs inverted by interaction. On the other hand, τ_c decreases with increasing r , causing significant reduction $\propto \tau^N$ of $|C_-(\tau)|^2$. The two processes compete, and in order to surpass the Bell limit, P_r has to be large enough. We note that R_r also plays a role in the above considerations, since the first term in the expansion of $|C_+|^2$, which leads to Gaussian decay, is insufficient to describe the violation of the Bell limit.

APPENDIX C: MEASURING MANY-BODY BELL CORRELATOR WITH THE MULTIPLE QUANTUM COHERENCES

The multiple quantum coherences (MQCs) technique provides extensive information about the structure of a many-body state. It allows for the relation of the quantum correlators with other physical quantities, such as the out-of-time-order correlations [91,92]. The MQC is defined upon picking some observable \hat{A} and expressing a density operator in terms of the eigenstates and eigenvalues of \hat{A} as follows:

$$\hat{\rho} = \sum_m \sum_{\lambda_i - \lambda_j = m} \varrho_{ij} |\psi_i\rangle \langle \psi_j| \equiv \sum_m \hat{\rho}_m, \quad (\text{C1})$$

where $\hat{A}|\psi_{i/j}\rangle = \lambda_{i/j}|\psi_{i/j}\rangle$. The MQC is defined as a norm of the fixed- m part of the density matrix, namely, $I_m(\hat{\rho}) = \text{Tr}[\hat{\rho}_m^\dagger \hat{\rho}_m]$. In the multiqubit case considered in the current work, we consider

$$\hat{A} = \frac{1}{2} \sum_{k=1}^N \hat{\sigma}_x^{(k)} \quad (\text{C2})$$

and $m = N/2$ to obtain

$$I_N(\hat{\rho}_{\text{out}}(\tau)) = \mathcal{E}_N(\tau). \quad (\text{C3})$$

The $I_N(\hat{\rho})$ is directly accessible in the laboratory, as shown in Ref. [91] for $N = 6$ qubits.

For a more detailed discussion of the physical significance of the MQCs, their measurements, and the relation to the out-of-time-order correlations, see Ref. [92] and references therein.

[1] A. Acín, I. Bloch, H. Buhrman, T. Calarco, C. Eichler, J. Eisert, D. Esteve, N. Gisin, S. J. Glaser, F. Jelezko, S. Kuhr, M. Lewenstein, M. F. Riedel, P. O. Schmidt, R. Thew, A. Wallraff, I. Walmsley, and F. K. Wilhelm, The quantum technologies roadmap: A European community view, *New J. Phys.* **20**, 080201 (2018).
[2] J. Eisert, D. Hangleiter, N. Walk, I. Roth, D. Markham, R. Parekh, U. Chabaud, and E. Kashefi, Quantum certification and benchmarking, *Nat. Rev. Phys.* **2**, 382 (2020).

[3] J. Fraxanet, T. Salamon, and M. Lewenstein, The coming decades of quantum simulation, in *Sketches of Physics* (Springer International Publishing, Cham, Switzerland, 2023), pp. 85–125.
[4] R. Horodecki, P. Horodecki, M. Horodecki, and K. Horodecki, Quantum entanglement, *Rev. Mod. Phys.* **81**, 865 (2009).
[5] R. Uola, A. C. S. Costa, H. C. Nguyen, and O. Gühne, Quantum steering, *Rev. Mod. Phys.* **92**, 015001 (2020).

- [6] N. Brunner, D. Cavalcanti, S. Pironio, V. Scarani, and S. Wehner, Bell nonlocality, *Rev. Mod. Phys.* **86**, 419 (2014).
- [7] I. Frérot, M. Fadel, and M. Lewenstein, Probing quantum correlations in many-body systems: A review of scalable methods, *Rep. Prog. Phys.* **86**, 114001 (2023).
- [8] M. Kitagawa and M. Ueda, Squeezed spin states, *Phys. Rev. A* **47**, 5138 (1993).
- [9] D. J. Wineland, J. J. Bollinger, W. M. Itano, and D. J. Heinzen, Squeezed atomic states and projection noise in spectroscopy, *Phys. Rev. A* **50**, 67 (1994).
- [10] L. Pezzè, A. Smerzi, M. K. Oberthaler, R. Schmied, and P. Treutlein, Quantum metrology with nonclassical states of atomic ensembles, *Rev. Mod. Phys.* **90**, 035005 (2018).
- [11] F. Wolfgramm, A. Cerè, F. A. Beduini, A. Predojević, M. Koschorreck, and M. W. Mitchell, Squeezed-light optical magnetometry, *Phys. Rev. Lett.* **105**, 053601 (2010).
- [12] G. Müller-Rigat, A. K. Srivastava, S. Kurdzialek, G. Rajchel-Międzioć, M. Lewenstein, and I. Frérot, Certifying the quantum Fisher information from a given set of mean values: A semidefinite programming approach, *Quantum* **7**, 1152 (2023).
- [13] J. Tura, R. Augusiak, A. B. Sainz, T. Vértesi, M. Lewenstein, and A. Acín, Detecting nonlocality in many-body quantum states, *Science* **344**, 1256 (2014).
- [14] R. Schmied, J.-D. Bancal, B. Allard, M. Fadel, V. Scarani, P. Treutlein, and N. Sangouard, Bell correlations in a Bose-Einstein condensate, *Science* **352**, 441 (2016).
- [15] A. Aloy, J. Tura, F. Baccari, A. Acín, M. Lewenstein, and R. Augusiak, Device-independent witnesses of entanglement depth from two-body correlators, *Phys. Rev. Lett.* **123**, 100507 (2019).
- [16] F. Baccari, J. Tura, M. Fadel, A. Aloy, J.-D. Bancal, N. Sangouard, M. Lewenstein, A. Acín, and R. Augusiak, Bell correlation depth in many-body systems, *Phys. Rev. A* **100**, 022121 (2019).
- [17] J. Tura, A. Aloy, F. Baccari, A. Acín, M. Lewenstein, and R. Augusiak, Optimization of device-independent witnesses of entanglement depth from two-body correlators, *Phys. Rev. A* **100**, 032307 (2019).
- [18] G. Müller-Rigat, A. Aloy, M. Lewenstein, and I. Frérot, Inferring nonlinear many-body Bell inequalities from average two-body correlations: Systematic approach for arbitrary spin- j ensembles, *PRX Quantum* **2**, 030329 (2021).
- [19] M. Żukowski and Č. Brukner, Bell's theorem for general n -qubit states, *Phys. Rev. Lett.* **88**, 210401 (2002).
- [20] E. G. Cavalcanti, C. J. Foster, M. D. Reid, and P. D. Drummond, Bell inequalities for continuous-variable correlations, *Phys. Rev. Lett.* **99**, 210405 (2007).
- [21] Q. Y. He, P. D. Drummond, and M. D. Reid, Entanglement, EPR steering, and Bell-nonlocality criteria for multipartite higher-spin systems, *Phys. Rev. A* **83**, 032120 (2011).
- [22] E. G. Cavalcanti, Q. Y. He, M. D. Reid, and H. M. Wiseman, Unified criteria for multipartite quantum nonlocality, *Phys. Rev. A* **84**, 032115 (2011).
- [23] A. Niezgodą, M. Panfil, and J. Chwedeńczuk, Quantum correlations in spin chains, *Phys. Rev. A* **102**, 042206 (2020).
- [24] A. Niezgodą and J. Chwedeńczuk, Many-body nonlocality as a resource for quantum-enhanced metrology, *Phys. Rev. Lett.* **126**, 210506 (2021).
- [25] J. Chwedeńczuk, Many-body Bell inequalities for bosonic qubits, *SciPost Phys. Core* **5**, 025 (2022).
- [26] D. J. Wineland, J. J. Bollinger, W. M. Itano, F. L. Moore, and D. J. Heinzen, Spin squeezing and reduced quantum noise in spectroscopy, *Phys. Rev. A* **46**, R6797 (1992).
- [27] K. Gietka, P. Szańkowski, T. Wasak, and J. Chwedeńczuk, Quantum-enhanced interferometry and the structure of twisted states, *Phys. Rev. A* **92**, 043622 (2015).
- [28] Y. Li, Y. Castin, and A. Sinatra, Optimum spin squeezing in Bose-Einstein condensates with particle losses, *Phys. Rev. Lett.* **100**, 210401 (2008).
- [29] Y. Li, P. Treutlein, J. Reichel, and A. Sinatra, Spin squeezing in a bimodal condensate: Spatial dynamics and particle losses, *Eur. Phys. J. B* **68**, 365 (2009).
- [30] M. Wang, W. Qu, P. Li, H. Bao, V. Vuletić, and Y. Xiao, Two-axis-twisting spin squeezing by multipass quantum erasure, *Phys. Rev. A* **96**, 013823 (2017).
- [31] D. Kajtoch, E. Witkowska, and A. Sinatra, Spin-squeezed atomic crystal, *Europhys. Lett.* **123**, 20012 (2018).
- [32] M. Schulte, C. Lisdat, P. O. Schmidt, U. Sterr, and K. Hammerer, Prospects and challenges for squeezing-enhanced optical atomic clocks, *Nat. Commun.* **11**, 5955 (2020).
- [33] K. Gietka, A. Usui, J. Deng, and T. Busch, Simulating the same physics with two distinct Hamiltonians, *Phys. Rev. Lett.* **126**, 160402 (2021).
- [34] T. Comparin, F. Mezzacapo, and T. Roscilde, Robust spin squeezing from the tower of states of $U(1)$ -symmetric spin Hamiltonians, *Phys. Rev. A* **105**, 022625 (2022).
- [35] M. F. Riedel, P. Böhi, Y. Li, T. W. Hänsch, A. Sinatra, and P. Treutlein, Atom-chip-based generation of entanglement for quantum metrology, *Nature (London)* **464**, 1170 (2010).
- [36] C. Gross, T. Zibold, E. Nicklas, J. Estève, and M. K. Oberthaler, Nonlinear atom interferometer surpasses classical precision limit, *Nature (London)* **464**, 1165 (2010).
- [37] C. D. Hamley, C. S. Gerving, T. M. Hoang, E. M. Bookjans, and M. S. Chapman, Spin-nematic squeezed vacuum in a quantum gas, *Nat. Phys.* **8**, 305 (2012).
- [38] A. Qu, B. Evrard, J. Dalibard, and F. Gerbier, Probing spin correlations in a Bose-Einstein condensate near the single-atom level, *Phys. Rev. Lett.* **125**, 033401 (2020).
- [39] I. D. Leroux, M. H. Schleier-Smith, and V. Vuletić, Implementation of cavity squeezing of a collective atomic spin, *Phys. Rev. Lett.* **104**, 073602 (2010).
- [40] K. Maussang, G. E. Marti, T. Schneider, P. Treutlein, Y. Li, A. Sinatra, R. Long, J. Estève, and J. Reichel, Enhanced and reduced atom number fluctuations in a BEC splitter, *Phys. Rev. Lett.* **105**, 080403 (2010).
- [41] A. Omran, H. Levine, A. Keesling, G. Semeghini, T. T. Wang, S. Ebadi, H. Bernien, A. S. Zibrov, H. Pichler, S. Choi, J. Cui, M. Rossignolo, P. Rembold, S. Montangero, T. Calarco, M. Endres, M. Greiner, V. Vuletić, and M. D. Lukin, Generation and manipulation of Schrödinger cat states in Rydberg atom arrays, *Science* **365**, 570 (2019).
- [42] G. Bornet, G. Emperauger, C. Chen, B. Ye, M. Block, M. Bintz, J. A. Boyd, D. Barredo, T. Comparin, F. Mezzacapo, T. Roscilde, T. Lahaye, N. Y. Yao, and A. Browaeys, Scalable spin squeezing in a dipolar Rydberg atom array, *Nature (London)* **621**, 728 (2023).
- [43] W. J. Eckner, N. Darkwah Oppong, A. Cao, A. W. Young, W. R. Milner, J. M. Robinson, J. Ye, and A. M. Kaufman, Realizing

- spin squeezing with Rydberg interactions in an optical clock, *Nature (London)* **621**, 734 (2023).
- [44] J. G. Bohnet, B. C. Sawyer, J. W. Britton, M. L. Wall, A. M. Rey, M. Foss-Feig, and J. J. Bollinger, Quantum spin dynamics and entanglement generation with hundreds of trapped ions, *Science* **352**, 1297 (2016).
- [45] J. Franke, S. R. Muleady, R. Kaubruegger, F. Kranzl, R. Blatt, A. M. Rey, M. K. Joshi, and C. F. Roos, Quantum-enhanced sensing on optical transitions through finite-range interactions, *Nature (London)* **621**, 740 (2023).
- [46] C. Song, K. Xu, W. Liu, C.-P. Yang, S.-B. Zheng, H. Deng, Q. Xie, K. Huang, Q. Guo, L. Zhang, P. Zhang, D. Xu, D. Zheng, X. Zhu, H. Wang, Y.-A. Chen, C.-Y. Lu, S. Han, and J.-W. Pan, 10-qubit entanglement and parallel logic operations with a superconducting circuit, *Phys. Rev. Lett.* **119**, 180511 (2017).
- [47] C. Song, K. Xu, H. Li, Y.-R. Zhang, X. Zhang, W. Liu, Q. Guo, Z. Wang, W. Ren, J. Hao, H. Feng, H. Fan, D. Zheng, D.-W. Wang, H. Wang, and S.-Y. Zhu, Generation of multicomponent atomic Schrödinger cat states of up to 20 qubits, *Science* **365**, 574 (2019).
- [48] K. Xu, Z.-H. Sun, W. Liu, Y.-R. Zhang, H. Li, H. Dong, W. Ren, P. Zhang, F. Nori, D. Zheng, H. Fan, and H. Wang, Probing dynamical phase transitions with a superconducting quantum simulator, *Sci. Adv.* **6**, eaba4935 (2020).
- [49] P. He, M. A. Perlin, S. R. Muleady, R. J. Lewis-Swan, R. B. Hutson, J. Ye, and A. M. Rey, Engineering spin squeezing in a 3D optical lattice with interacting spin-orbit-coupled fermions, *Phys. Rev. Res.* **1**, 033075 (2019).
- [50] M. Płodzień, M. Kościelski, E. Witkowska, and A. Sinatra, Producing and storing spin-squeezed states and Greenberger-Horne-Zeilinger states in a one-dimensional optical lattice, *Phys. Rev. A* **102**, 013328 (2020).
- [51] M. Płodzień, M. Lewenstein, E. Witkowska, and J. Chwedeńczuk, One-axis twisting as a method of generating many-body Bell correlations, *Phys. Rev. Lett.* **129**, 250402 (2022).
- [52] M. Mamaev, I. Kimchi, R. M. Nandkishore, and A. M. Rey, Tunable-spin-model generation with spin-orbit-coupled fermions in optical lattices, *Phys. Rev. Res.* **3**, 013178 (2021).
- [53] T. H. Yanes, M. Płodzień, M. M. Sinkevičienė, G. Žlabys, G. Juzeliūnas, and E. Witkowska, One- and two-axis squeezing via laser coupling in an atomic Fermi-Hubbard model, *Phys. Rev. Lett.* **129**, 090403 (2022).
- [54] M. Dziurawiec, T. H. Yanes, M. Płodzień, M. Gajda, M. Lewenstein, and E. Witkowska, Accelerating many-body entanglement generation by dipolar interactions in the Bose-Hubbard model, *Phys. Rev. A* **107**, 013311 (2023).
- [55] T. H. Yanes, G. Žlabys, M. Płodzień, D. Burba, M. M. Sinkevičienė, E. Witkowska, and G. Juzeliūnas, Spin squeezing in open Heisenberg spin chains, *Phys. Rev. B* **108**, 104301 (2023).
- [56] L. K. Joshi, A. Elben, A. Vikram, B. Vermersch, V. Galitski, and P. Zoller, Probing many-body quantum chaos with quantum simulators, *Phys. Rev. X* **12**, 011018 (2022).
- [57] C. Kokail, R. van Bijnen, A. Elben, B. Vermersch, and P. Zoller, Entanglement Hamiltonian tomography in quantum simulation, *Nat. Phys.* **17**, 936 (2021).
- [58] S. Hollerith, K. Srakaew, D. Wei, A. Rubio-Abadal, D. Adler, P. Weckesser, A. Kruckenhauser, V. Walther, R. van Bijnen, J. Rui, C. Gross, I. Bloch, and J. Zeiher, Realizing distance-selective interactions in a Rydberg-dressed atom array, *Phys. Rev. Lett.* **128**, 113602 (2022).
- [59] Q. Y. He, E. G. Cavalcanti, M. D. Reid, and P. D. Drummond, Bell inequalities for continuous-variable measurements, *Phys. Rev. A* **81**, 062106 (2010).
- [60] U. Leonhardt, Quantum-state tomography and discrete Wigner function, *Phys. Rev. Lett.* **74**, 4101 (1995).
- [61] A. G. White, D. F. V. James, P. H. Eberhard, and P. G. Kwiat, Nonmaximally entangled states: Production, characterization, and utilization, *Phys. Rev. Lett.* **83**, 3103 (1999).
- [62] C. F. Roos, G. P. T. Lancaster, M. Riebe, H. Häffner, W. Hänsel, S. Gulde, C. Becher, J. Eschner, F. Schmidt-Kaler, and R. Blatt, Bell states of atoms with ultralong lifetimes and their tomographic state analysis, *Phys. Rev. Lett.* **92**, 220402 (2004).
- [63] H. Häffner, W. Hänsel, C. F. Roos, J. Benhelm, D. Chek-al kar, M. Chwalla, T. Körber, U. D. Rapol, M. Riebe, P. O. Schmidt, C. Becher, O. Gühne, W. Dür, and R. Blatt, Scalable multiparticle entanglement of trapped ions, *Nature (London)* **438**, 643 (2005).
- [64] D. Gross, Recovering low-rank matrices from few coefficients in any basis, *IEEE Trans. Inf. Theory* **57**, 1548 (2011).
- [65] G. Tóth, W. Wieczorek, D. Gross, R. Krischek, C. Schwemmer, and H. Weinfurter, Permutationally invariant quantum tomography, *Phys. Rev. Lett.* **105**, 250403 (2010).
- [66] T. Moroder, P. Hyllus, G. Tóth, C. Schwemmer, A. Niggebaum, S. Gaile, O. Gühne, and H. Weinfurter, Permutationally invariant state reconstruction, *New J. Phys.* **14**, 105001 (2012).
- [67] M. Cramer, M. B. Plenio, S. T. Flammia, R. Somma, D. Gross, S. D. Bartlett, O. Landon-Cardinal, D. Poulin, and Y.-K. Liu, Efficient quantum state tomography, *Nat. Commun.* **1**, 149 (2010).
- [68] T. Baumgratz, D. Gross, M. Cramer, and M. B. Plenio, Scalable reconstruction of density matrices, *Phys. Rev. Lett.* **111**, 020401 (2013).
- [69] B. P. Lanyon, C. Maier, M. Holzäpfel, T. Baumgratz, C. Hempel, P. Jurcevic, I. Dhand, A. S. Buyskikh, A. J. Daley, M. Cramer, M. B. Plenio, R. Blatt, and C. F. Roos, Efficient tomography of a quantum many-body system, *Nat. Phys.* **13**, 1158 (2017).
- [70] A. Palmieri, E. Kovlakov, F. Bianchi, D. Yudin, S. Straupe, J. D. Biamonte, and S. Kulik, Experimental neural network enhanced quantum tomography, *npj Quantum Inf.* **6**, 20 (2020).
- [71] C. Pan and J. Zhang, Deep learning-based quantum state tomography with imperfect measurement, *Int. J. Theor. Phys.* **61**, 227 (2022).
- [72] D. Koutný, L. Motka, Z. Hradil, J. Řeháček, and L. L. Sánchez-Soto, Neural-network quantum state tomography, *Phys. Rev. A* **106**, 012409 (2022).
- [73] S. Ahmed, C. Sánchez Muñoz, F. Nori, and A. F. Kockum, Quantum state tomography with conditional generative adversarial networks, *Phys. Rev. Lett.* **127**, 140502 (2021).
- [74] H. Ma, Z. Sun, D. Dong, C. Chen, and H. Rabitz, Attention-based transformer networks for quantum state tomography, *arXiv:2305.05433*.
- [75] A. M. Palmieri, G. Müller-Rigat, A. K. Srivastava, M. Lewenstein, G. Rajchel-Mieldzioć, and M. Płodzień, Enhancing quantum state tomography via resource-efficient attention-based neural networks, *arXiv:2309.10616*.
- [76] A. Dawid, J. Arnold, B. Requena, A. Gresch, M. Płodzień, K. Donatella, K. A. Nicoli, P. Stornati, R. Koch, M. Büttner, R.

- Okuła, G. Muñoz-Gil, R. A. Vargas-Hernández, A. Cervera-Lierta, J. Carrasquilla, V. Dunjko, M. Gabrié, P. Huembeli, E. van Nieuwenburg, F. Vicentini *et al.*, Modern applications of machine learning in quantum sciences, [arXiv:2204.04198](https://arxiv.org/abs/2204.04198).
- [77] S. Aaronson and G. N. Rothblum, Gentle measurement of quantum states and differential privacy, in *Proceedings of the 51st Annual ACM SIGACT Symposium on Theory of Computing, STOC 2019* (Association for Computing Machinery, New York, NY, USA, 2019), pp. 322–333.
- [78] H.-Y. Huang, R. Kueng, and J. Preskill, Predicting many properties of a quantum system from very few measurements, *Nat. Phys.* **16**, 1050 (2020).
- [79] J. B. Altepeter, D. F. James, and P. G. Kwiat, 4 qubit quantum state tomography, *Quantum state estimation, Lect. Notes Phys.* **649**, 113 (2004).
- [80] J. Haah, A. W. Harrow, Z. Ji, X. Wu, and N. Yu, Sample-optimal tomography of quantum states, *IEEE Trans. Inf. Theory* **63**, 5628 (2017).
- [81] R. O’Donnell and J. Wright, Efficient quantum tomography, in *Proceedings of the Forty-Eighth Annual ACM Symposium on Theory of Computing, STOC’16* (Association for Computing Machinery, New York, NY, USA, 2016), pp. 899–912.
- [82] D. E. Koh and S. Grewal, Classical shadows with noise, *Quantum* **6**, 776 (2022).
- [83] S. Aaronson, Shadow tomography of quantum states, *Proceedings of the 50th annual ACM SIGACT symposium on theory of computing* (2018), pp. 325–338.
- [84] A. Elben, R. Kueng, H.-Y. R. Huang, R. van Bijnen, C. Kokail, M. Dalmonte, P. Calabrese, B. Kraus, J. Preskill, P. Zoller, and B. Vermersch, Mixed-state entanglement from local randomized measurements, *Phys. Rev. Lett.* **125**, 200501 (2020).
- [85] H.-Y. Huang, R. Kueng, and J. Preskill, Efficient estimation of Pauli observables by derandomization, *Phys. Rev. Lett.* **127**, 030503 (2021).
- [86] A. Elben, S. T. Flammia, H.-Y. Huang, R. Kueng, J. Preskill, B. Vermersch, and P. Zoller, The randomized measurement toolbox, *Nat. Rev. Phys.* **5**, 9 (2023).
- [87] M. McGinley and M. Fava, Shadow tomography from emergent state designs in analog quantum simulators, *Phys. Rev. Lett.* **131**, 160601 (2023).
- [88] M. C. Tran, D. K. Mark, W. W. Ho, and S. Choi, Measuring arbitrary physical properties in analog quantum simulation, *Phys. Rev. X* **13**, 011049 (2023).
- [89] B. P. Lanyon, C. Hempel, D. Nigg, M. Müller, R. Gerritsma, F. Zähringer, P. Schindler, J. T. Barreiro, M. Rambach, G. Kirchmair, M. Hennrich, P. Zoller, R. Blatt, and C. F. Roos, Universal digital quantum simulation with trapped ions, *Science* **334**, 57 (2011).
- [90] S. Notarnicola, A. Elben, T. Lahaye, A. Browaeys, S. Montangero, and B. Vermersch, A randomized measurement toolbox for an interacting Rydberg-atom quantum simulator, *New J. Phys.* **25**, 103006 (2023).
- [91] M. Gärttner, J. G. Bohnet, A. Safavi-Naini, M. L. Wall, J. J. Bollinger, and A. M. Rey, Measuring out-of-time-order correlations and multiple quantum spectra in a trapped-ion quantum magnet, *Nat. Phys.* **13**, 781 (2017).
- [92] M. Gärttner, P. Hauke, and A. M. Rey, Relating out-of-time-order correlations to entanglement via multiple-quantum coherences, *Phys. Rev. Lett.* **120**, 040402 (2018).
- [93] Z.-H. Sun, Y.-Y. Wang, Y.-R. Zhang, F. Nori, and H. Fan, Variational generation of spin squeezing on one-dimensional quantum devices with nearest-neighbor interactions, *Phys. Rev. Res.* **5**, 043285 (2023).
- [94] Y. Li and S. C. Benjamin, One-dimensional quantum computing with a ‘segmented chain’ is feasible with today’s gate fidelities, *npj Quantum Inf.* **4**, 25 (2018).
- [95] Details of analytical derivation and a numerical code used for obtaining the Bell correlator for concrete values of N and r are available at the following address: <https://github.com/mplodzien/Many-body-quantum-correlations-in-spin-chains>.
- [96] M. Płodzień, T. Wasak, E. Witkowska, M. Lewenstein, J. Chwedeńczuk, Datasets for “Generation of scalable many-body Bell correlations in spin chains with short-range two-body interactions” (RepOD, 2024), doi: [10.18150/XLEKW5](https://doi.org/10.18150/XLEKW5).